



Article

Effects of Fe, Mn Individual Doping and (Fe, Mn) Co-Doping on Ferromagnetic Properties of Co₂Si Powders

Jiang Zou ^{1,2}, Lifeng Wang ², Juan He ², Bo Wu ² and Quan Xie ^{1,*}

¹ College of Big Data and Information Engineering, Guizhou University, Guiyang 550025, China; yywanj1@163.com

² School of Physics and Electronic Science, Zunyi Normal College, Zunyi 563006, China; wlf1234560116@163.com (L.W.); hejuan0209@126.com (J.H.); fqwubo@163.com (B.W.)

* Correspondence: qxie@gzu.edu.cn

Abstract: Magnetic materials are crucial energy materials that are widely used in day-to-day life. Therefore, the development and study of high-performance magnetic materials are of great significance. In this study, the magnetic materials Co_{66.6}Si_{33.4}, Co_{60.6}X₆Si_{33.4} (X = Fe, Mn), and Co_{60.6}Fe₃Mn₃Si_{33.4} were prepared via the ball milling and sintering processes. Their crystal structures, electrical conductivity, and magnetic properties were investigated via the X-ray diffraction analysis and by using a resistivity tester, vibrating sample magnetometer, and vector network analyser. The X-ray diffraction analysis revealed that a single phase of Co_{66.6}Si_{33.4} and its doped alloy powders were successfully obtained. The electrical conductivities of Mn₆Co_{60.6}Si_{33.4} and Fe₃Mn₃Co_{60.6}Si_{33.4} were measured using a resistivity tester. The results indicate that Mn doping and Fe and Mn Co-doping enhanced the electrical conductivity of Co_{66.6}Si_{33.4}. The magnetic properties of Co_{66.6}Si_{33.4} were determined using a vibrating sample magnetometer. We observed that the magnetic properties were enhanced after doping. Co_{60.6}Fe₃Mn₃Si_{33.4} exhibited excellent magnetic properties. Further, its permeability was determined using a vector network analyser. At a low frequency, the u' and u'' values of Co_{60.6}Fe₆Si_{33.4} and Co_{60.6}Fe₃Mn₃Si_{33.4} were enhanced; whereas, at a high frequency, after doping, the u' and u'' values changed only slightly. This study can be used as a basis for future studies on magnetic functional materials.

Keywords: magnetic; doping; Co₂Si; saturation magnetisation; coercivity; remanence



Citation: Zou, J.; Wang, L.; He, J.; Wu, B.; Xie, Q. Effects of Fe, Mn Individual Doping and (Fe, Mn) Co-Doping on Ferromagnetic Properties of Co₂Si Powders. *Nanomaterials* **2022**, *12*, 293. <https://doi.org/10.3390/nano12020293>

Academic Editor: Jan Macutkevicius

Received: 25 November 2021

Accepted: 11 January 2022

Published: 17 January 2022

Publisher's Note: MDPI stays neutral with regard to jurisdictional claims in published maps and institutional affiliations.



Copyright: © 2022 by the authors. Licensee MDPI, Basel, Switzerland. This article is an open access article distributed under the terms and conditions of the Creative Commons Attribution (CC BY) license (<https://creativecommons.org/licenses/by/4.0/>).

1. Introduction

Magnetic materials are widely used in various fields of renewable energy, energy conservation and environmental protection, such as solar and wind power generation, new energy vehicles, rail transit, energy saving lighting, and new planar displays [1–3]. Presently, the intermetallic compound Co–Si is an important alloy widely used in the fields of electronics, power, and machinery [4,5]. It has good oxidation and corrosion resistances, stable physical and chemical properties, high temperature resistance, high strength, a large elastic modulus, and high structural stability [6]. It has the potential to be used as a high-temperature structural material.

Chuan et al. [7] prepared CoSi by mechanical alloying and performed thermodynamic analysis. They observed that metallic compounds were initially formed. PanzhiJun et al. [8] studied the thermoelectric properties of CoSi. Joa et al. investigated the magnetic properties of Co–Si alloy clusters. The electronic structure and magnetic properties of the Co–Si alloy clusters were investigated using ab initio spin-polarised density functional calculations. The magnetic moment primarily depended on the Co–Si bond lengths rather than the Co–Co bond lengths [9].

Velez and Valvidares conducted a study on the structural and magnetic properties of amorphous Co–Si alloy films. The results showed that the heterogeneity of the high Co content led to an essentially isotropic magnetic behaviour and the formation of highly coercive fields [10].

Geller synthesized single-phase Co_2Si by mechanical ball milling and heat treatment and determined its crystal structure and magnetic properties [11]. China-hong investigated the following three intermediate phases: Co_2Si , CoSi , and CoSi_2 . The results showed that CoSi , Co_2Si , and CoSi_2 were found in these couples when the bulks were annealed at temperatures of 800, 900, 1000, and 1050 °C [12]. Cristina Bormio-Nunes studied the magnetisation of the Co–Si–B system. The results of the study showed that Co_2Si is paramagnetic [13].

Tu et al. investigated the thermal stability and growth kinetics of Co_2Si and CoSi in thin-film reactions. The results showed that a sequential growth of Co_2Si and CoSi was observed in the reaction between the Si and Co films. First, Co_2Si was formed, and, subsequently, CoSi was formed when all of the Co was consumed [14]. Baldan et al. investigated the microstructural evidence of β Co_2Si -phase stability in the Co–Si System. The stability of the β Co_2Si phase in the Co–Si system was verified [15].

Vander Walls-Zeeman studied the atomically disordered nanocrystalline compound Co_2Si prepared via high-energy ball milling. The results indicated anti-site disorder. Moreover, the continuous increase in the rate of magnetisation confirmed the generation of the anti-site disorder in Co_2Si [16].

However, studies on enhancing the magnetic properties of Co_2Si by doping have not been reported thus far. In this study, Co_2Si was prepared by ball milling with Fe and Mn as dopants and, Fe and Mn as co-dopants. The improvements in its magnetic properties were investigated.

2. Experimental Details

$\text{Co}_{66.6}\text{Si}_{33.4}$, $\text{Co}_{60.6}\text{X}_6\text{Si}_{33.4}$ (X = Fe, Mn), and $\text{Co}_{60.6}\text{Fe}_3\text{Mn}_3\text{Si}_{33.4}$ were prepared using Co, Si, Fe, and Mn powders with purity of 99.9% according to their molar fractions [17]. This method can only be used for inactive metals at room temperature to prevent severe oxidation in a short time. The powders after accurate weighing were placed in a stainless steel tank for ball milling. An OECO-PBM-AD-6L omni-directional ball mill manufactured by Hunan Deke was used to mill the powder. The samples were added with a ball-to-powder weight ratio of 40:1, and milling was performed for a duration of 72 h.

The rotational speed of the ball milling machine was maintained at 360 rpm. To prevent oxidation during ball milling, the stainless-steel tank was evacuated insert and pressed into a pellet [18]. Furthermore, close attention had to be paid to the sealing of the steel tank to prevent air leakage. The alloy powder obtained by ball milling was annealed at 950 °C for 2 h in a GSL-1500X tube furnace (Hefei Kejing Material Technology Co, Ltd. He Fei, Anhui, China), which incorporates a double layer air cooling structure to sinter samples.

The maximum sintering temperature of GSL-1500X tube furnace was 1500 °C. The structure of the sintered samples was characterised by X-ray diffraction (XRD, BRUKER D8 ADVANCE (Zhongguancun, Beijing, China), which is produced by the technology company BRUKER [19] to detect the phase of the material. To ensure the accuracy of the diffraction data, first, the sample was ground into a powder suitable for the diffraction experiment; subsequently, sample powder was transformed into a flat test piece.

The hysteresis loop of each samples was measured using a vibrating sample magnetometer (VSM, Lakeshore7404, Baoshan District, Shanghai, China) [20]. When the hysteresis loop of a nanomagnetic material was being tested, as the material had a considerably small particle size and rich surface, the magnetisation of the surface magnetic moment of the magnetic particle was difficult to measure due to its high energy. This led to the hysteresis loop not being sufficiently stable in a high magnetic field.

Generally, the magnetisation corresponding to the maximum magnetic field is considered the saturation magnetisation of such materials. The permeability was determined using the vector network analyser (Agilent, Chaoyang District, Beijing, China) [21]. The coaxial method is the most suitable for powders and the waveguide method is primarily suitable for resins. In the course of measurement, a coaxial ring was made of powder and paraffin. The concentration ratio of sample to paraffin was 40:60. The conductivity

of the samples was measured using a high-precision resistivity tester (YAOS, Guangzhou, Guangdong, China) [22].

The powder micrograph images were tested by transmission electron microscopy (TEM; Tecnai G2 F20, Fei Company, Hillsboro, OR, USA) [23]. The TEM test showed the micrograph images and grain size on the nanoscale. The sample comprised organic or magnetic matter; therefore, the turbulence under high pressure was more severe. Consequently, it was difficult to capture a good effect, leading to errors.

3. Results and Discussion

Figure 1 shows the XRD pattern of mechanically alloyed powder after sintering at 950 °C. All the highly intense peaks match those of the diffraction pattern of Co_2Si with the crystal system of orthorhombic (pdfcard98-005-2281).

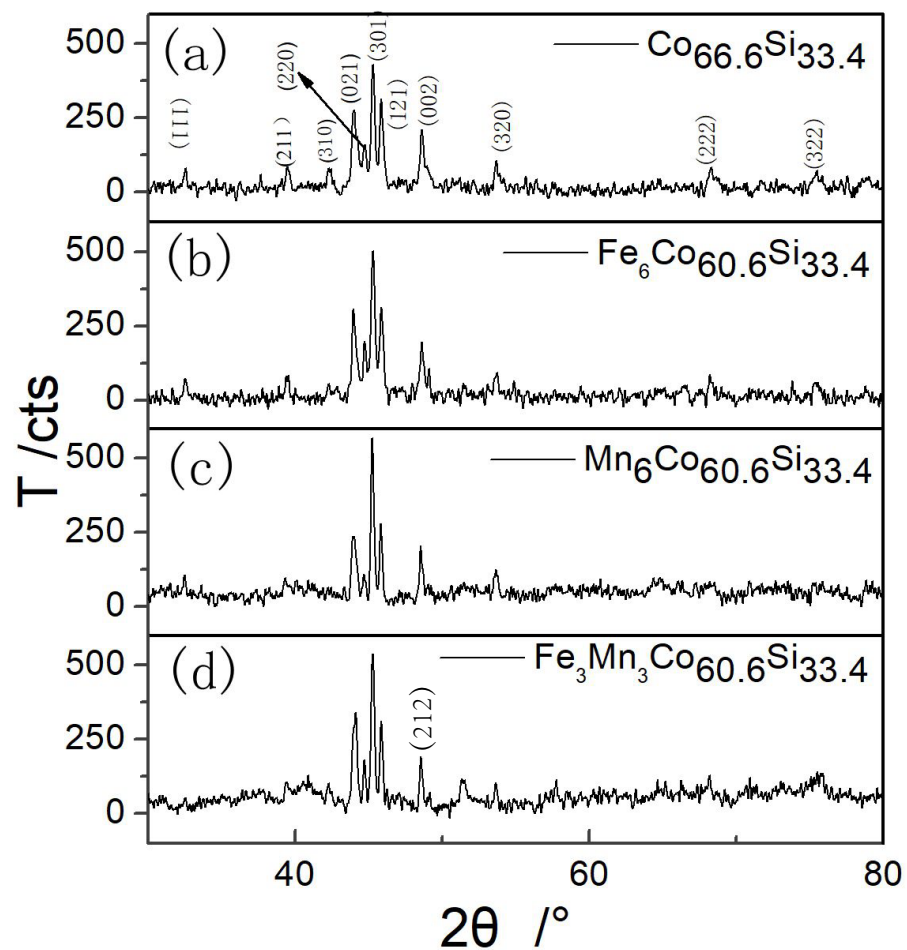


Figure 1. XRD patterns of (a) as-prepared $\text{Co}_{66.6}\text{Si}_{33.4}$, (b) Fe doped $\text{Co}_{66.6}\text{Si}_{33.4}$, (c) Mn doped $\text{Co}_{66.6}\text{Si}_{33.4}$ and (d) Fe and Mn co-doped $\text{Co}_{66.6}\text{Si}_{33.4}$.

As shown in Figure 1, highly intense diffraction peaks were observed corresponding to (021), (301) and (121) planes. From the XRD pattern of $\text{Co}_{66.6}\text{Si}_{33.4}$ shown in Figure 1a, no diffraction peaks of Co and Si appeared after sintering the samples at 950 °C, indicating that the synthesized powder comprised a single $\text{Co}_{66.6}\text{Si}_{33.4}$ phase after mechanical alloying and heat treatment. Figure 1b–d shows the XRD patterns of $\text{X}_6\text{Co}_{60.6}\text{Si}_{33.4}$ ($\text{X} = \text{Fe}, \text{Mn}$), and $\text{Fe}_3\text{Mn}_3\text{Co}_{60.6}\text{Si}_{33.4}$, respectively. The phase of $\text{Co}_{66.6}\text{Si}_{33.4}$ was observed by XRD. The Fe–Mn phase was not observed in the doped samples, as shown in Figure 1b–d, indicating that doping did not form other phases except the phase of $\text{Co}_{66.6}\text{Si}_{33.4}$. The diffraction peaks of (111), (211), and (310) at 32.593°, 39.459°, and 42.303°, respectively, observed for $\text{Co}_{66.6}\text{Si}_{33.4}$, were not present for $\text{Co}_{60.6}\text{Fe}_3\text{Mn}_3\text{Si}_{33.4}$.

In contrast, the diffraction peaks of (212) and (122) appeared at 51.327° and 58.850° for $\text{Co}_{60.6}\text{Fe}_3\text{Mn}_3\text{Si}_{33.4}$. These observations indicated that the doping of Mn and Fe-Mn slightly changed the preferred orientation. Table 1 shows different values of $2\theta^\circ$, the error between the measured and standard diffraction angle (B), the crystallographic inter-planar spacing (d), and the lattice constants of the corresponding crystal plane (a, b, and c). B and d were obtained by the XRD analysis.

By importing the detected data of the XRD, the lattice parameters of the crystal planes were calculated using JADE6.5 [24], which is an XRD analysis software. This software performs various functions, including XRD analysis of a given material, and analysis of its lattice parameters, FWHM (the half-width height of diffraction peak), and grain size. The diffraction peaks within the 2θ range from 41° to 51° were fitted using the Pearson-VII function [25]. The crystal sizes were obtained using the Scherrer formula and the Williamson–Hall method [26]. The calculation is as follows:

$$\beta_{hkl} = \beta_s - \beta_D \quad (1)$$

$$\beta_{hkl} = \left(\frac{k\lambda}{D \cos \theta} \right) + 4\epsilon \tan \theta \quad (2)$$

$$\beta_s = 4\epsilon \tan \theta \quad (3)$$

where D is the grain size in nanometres, β_{hkl} is the total broadening, λ is the wavelength of the radiation, k is a constant equal to 0.94, ϵ is the strain, β_D is the peak width at half-maximum intensity, and θ is the peak position.

Table 1. Lattice parameters of as-prepared $\text{Co}_{66.6}\text{Si}_{33.4}$, $\text{Co}_{60.6}\text{X}_6\text{Si}_{33.4}$, ($X = \text{Fe}, \text{Mn}$), and $\text{Co}_{60.6}\text{Fe}_3\text{Mn}_3\text{Si}_{33.4}$.

	$2\theta^\circ$	B	d (Å)	hkl	a (Å)	b (Å)	c (Å)
$\text{Co}_{66.6}\text{Si}_{33.4}$	43.899	0.242	2.0545	021	0.70813	0.49439	0.37311
	45.859	0.028	1.9999	301	0.70813	0.48499	0.37734
	45.277	0.115	1.9771	121	0.78013	0.49361	0.37394
$\text{Fe}_6\text{Co}_{60.6}\text{Si}_{33.4}$	43.902	0.239	2.0606	021	0.71019	0.49337	0.37480
	45.308	0.003	1.9999	301	0.71019	0.49582	0.37480
	45.874	0.100	1.9765	121	0.71019	0.49210	0.37536
$\text{Mn}_6\text{Co}_{66.6}\text{Si}_{33.4}$	44.002	0.139	2.0562	021	0.71639	0.49615	0.36752
	45.248	0.057	2.0024	301	0.71639	0.49615	0.36752
	45.877	0.097	1.9764	121	0.71639	0.49615	0.36752
$\text{Fe}_3\text{Mn}_3\text{Co}_{60.6}\text{Si}_{33.4}$	44.107	0.034	2.0510	021	0.71273	0.49225	0.37100
	45.413	0.108	2.0252	301	0.71273	0.49225	0.37100
	45.865	0.109	2.0007	121	0.71273	0.49225	0.37100

Figure 2a shows that the FWHM of the diffraction peaks for each sample were obtained within 41–51° using JADE6.5. Figure 2b shows the average grain size calculated using the Williamson–Hall method. Samples of about 1 g were applied to the glass for XRD and smoothed. The data of the samples obtained were imported into JADE. Then the diffraction peaks, (021), (220), (301), (121), and (002), were selected to calculate its grain size due to the major contribution of grain size. The calculated average grain size was 36.8 nm for $\text{Co}_{66.6}\text{Si}_{33.4}$, and the grain size changed after doping. This indicates that doping had an influence on the growth of the grain.

According to Table 2, the measured average grain sizes were 23, 21, 38, and 32 nm, for $\text{Co}_{66.6}\text{Si}_{33.4}$, $\text{Co}_{60.6}\text{X}_6\text{Si}_{33.4}$ ($X = \text{Fe}, \text{Mn}$), and $\text{Co}_{60.6}\text{Fe}_3\text{Mn}_3\text{Si}_{33.4}$, respectively. When the XRD was performed, the amount of powder was relatively large, about 1 g. In the XRD analysis. When TEM is made, only a small particle is taken about a few milligrams. Therefore, there was a certain error between the measured and estimated values.

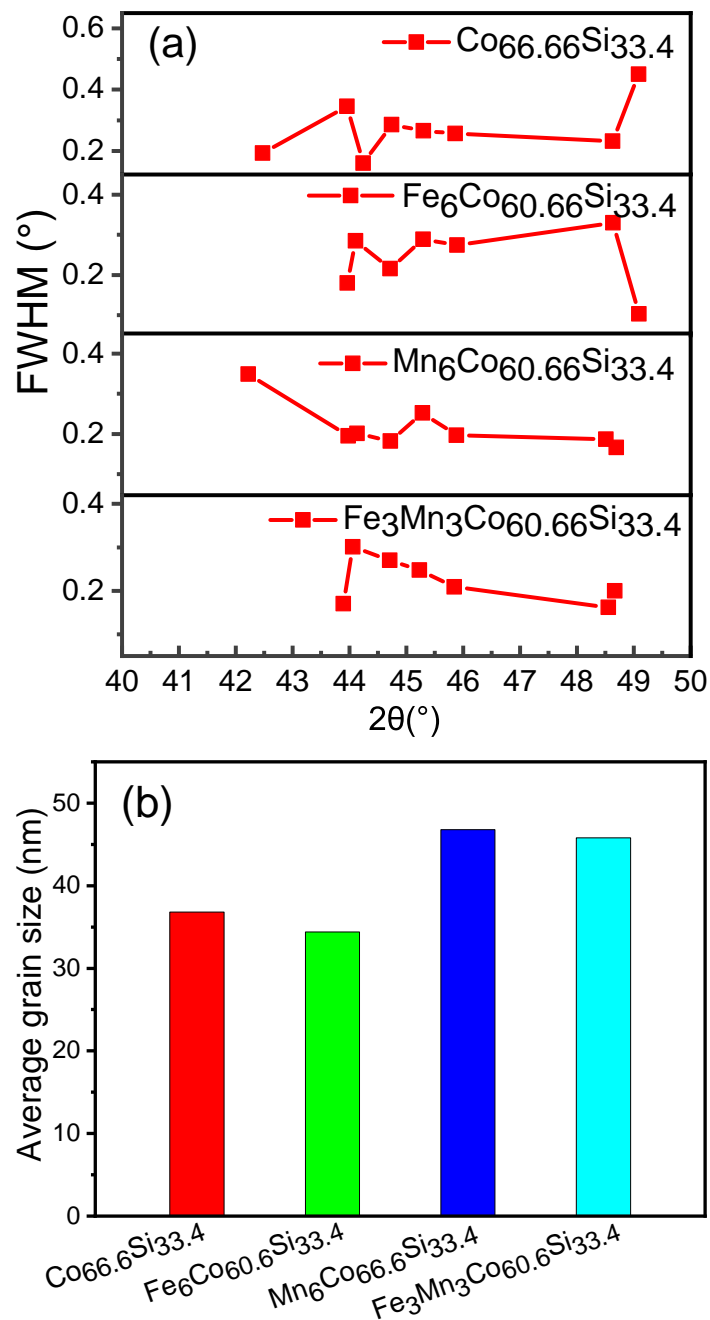


Figure 2. (a) FWHM of $\text{Co}_{66.6}\text{Si}_{33.4}$, $\text{Co}_{60.6}\text{X}_6\text{Si}_{33.4}$, ($\text{X} = \text{Fe}, \text{Mn}$), and $\text{Co}_{60.6}\text{Fe}_3\text{Mn}_3\text{Si}_{33.4}$; (b) Average grain size of as-prepared $\text{Co}_{66.6}\text{Si}_{33.4}$, $\text{Co}_{60.6}\text{X}_6\text{Si}_{33.4}$, ($\text{X} = \text{Fe}, \text{Mn}$), and $\text{Co}_{60.6}\text{Fe}_3\text{Mn}_3\text{Si}_{33.4}$.

A magnetic material affects the accuracy of the testing equipment, which is one of the reasons for the error. Figure 3a–d shows the powder micrograph images of $\text{Co}_{66.6}\text{Si}_{33.4}$, $\text{Co}_{60.6}\text{X}_6\text{Si}_{33.4}$ ($\text{X} = \text{Fe}, \text{Mn}$), and $\text{Co}_{60.6}\text{Fe}_3\text{Mn}_3\text{Si}_{33.4}$. The scale bar in Figure 3a–d equals 200 nm. The radii of Fe and Mn atoms are not greatly different from that of Co atoms. Hence, Fe and Mn atoms can enter the Co_2Si lattice and replace the Co atoms. In the periodic table, Fe and Co are adjacent to each other.

Therefore, when Fe atoms replace the Co atoms, they have little effect on the lattice growth compared to Mn atom doping. As the radii of Fe atoms and Co atoms are not very different, the diffusion is slow during the heating process, thereby, hindering the growth of the grain. The radius of Mn is smaller than that of Fe; therefore, it is easier to enter the Co_2Si lattice. Therefore, Mn doping and Fe–Mn doping promote growth of the grain.

Table 2. Average grain size by testing of as-prepared $\text{Co}_{66.6}\text{Si}_{33.4}$, $\text{Co}_{60.6}\text{X}_6\text{Si}_{33.4}$, ($\text{X} = \text{Fe}, \text{Mn}$), and $\text{Co}_{60.6}\text{Fe}_3\text{Mn}_3\text{Si}_{33.4}$.

Structure	$\text{Co}_{66.6}\text{Si}_{33.4}$	$\text{Fe}_6\text{Co}_{60.6}\text{Si}_{33.4}$	$\text{Mn}_6\text{Co}_{66.6}\text{Si}_{33.4}$	$\text{Fe}_3\text{Mn}_3\text{Co}_{60.6}\text{Si}_{33.4}$
Size (nm)	23	21	38	32

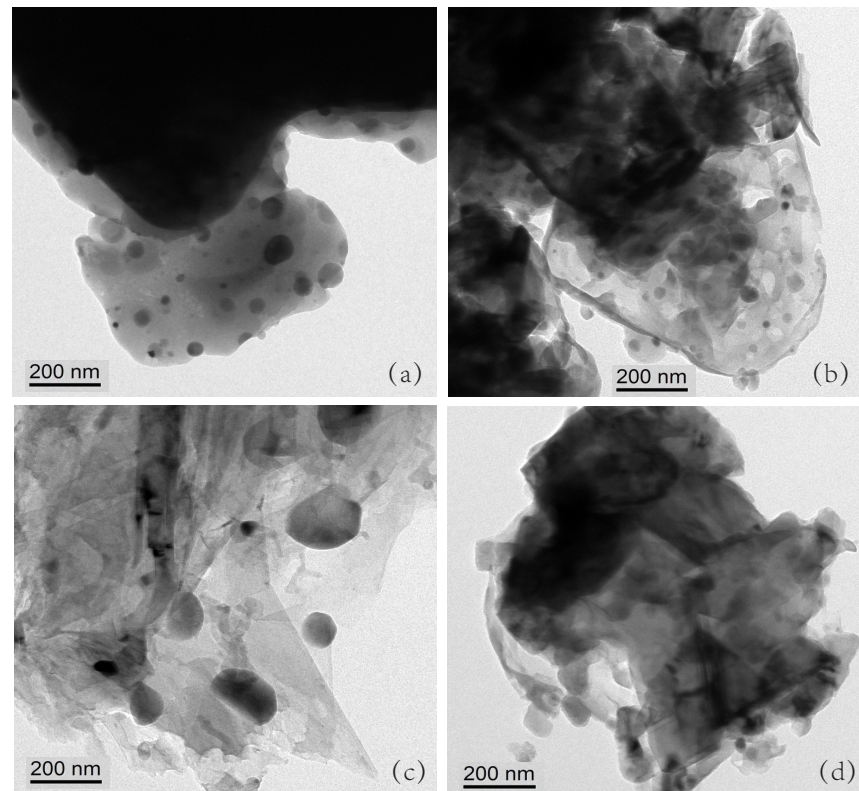
**Figure 3.** (a–d) Powder micrograph images of $\text{Co}_{66.6}\text{Si}_{33.4}$, $\text{Co}_{60.6}\text{X}_6\text{Si}_{33.4}$, ($\text{X} = \text{Fe}, \text{Mn}$), and $\text{Co}_{60.6}\text{Fe}_3\text{Mn}_3\text{Si}_{33.4}$.

Table 3 shows the conductivities of the as-prepared $\text{Co}_{66.6}\text{Si}_{33.4}$, $\text{Co}_{60.6}\text{X}_6\text{Si}_{33.4}$ ($\text{X} = \text{Fe}, \text{Mn}$), and $\text{Co}_{60.6}\text{Fe}_3\text{Mn}_3\text{Si}_{33.4}$. To study the effect of doping on the conductivities of the as-prepared $\text{Co}_{66.6}\text{Si}_{33.4}$ and doped $\text{Co}_{66.6}\text{Si}_{33.4}$, the resistivities of the samples were measured using a high-precision resistivity tester. Each sample was placed inside the sample pool, and a certain pressure was applied to the sample. The current and voltage parameters were set, and the high-precision resistivity tester was used to record the data. Under different pressures, the resistivities recorded were different; thus, we selected three different pressures. A resistance meter was used to measure their resistivities under the pressures of 1, 2, and 3 MPa.

The conductivity was calculated by taking the reciprocals of resistivities. As shown in Table 3, we chose 3 MPa as an example because the compounds followed the same rules under this pressure. Under 3 MPa, the conductivity of $\text{Co}_{66.6}\text{Si}_{33.4}$ was 183 S/m, which is very low. The conductivity of $\text{Fe}_6\text{Co}_{60.6}\text{Si}_{33.4}$ was 190 S/m, which indicates that the effect of Fe doping on its conductivity is insignificant.

The conductivities of $\text{Mn}_6\text{Co}_{60.6}\text{Si}_{33.4}$ and $\text{Fe}_3\text{Mn}_3\text{Co}_{60.6}\text{Si}_{33.4}$ were 111,000 and 32,000 S/m, indicating that Mn doping and Fe, Mn co-doping enhance the conductivity of $\text{Co}_{66.6}\text{Si}_{33.4}$. Conductivity is mainly determined by electron mobility. After sintering to form Co_2Si , the Co–Si bonding with electrons becomes relatively strong, resulting in a low conductivity.

After doping, the outermost layer of the 4d orbital of the Fe atom contains six electrons, whereas that of the 4d orbital of the Mn atom contains five electrons. Further, it is easier to lose a single electron from the outermost layer of the 4d orbital than to lose two electrons.

Therefore, the influence of Mn doping on improving the conductivity is significant, while that of Fe doping is relatively small.

Figure 4a–e shows the hysteresis loops of $\text{Co}_{66.6}\text{Si}_{33.4}$, $\text{Co}_{60.6}\text{X}_6\text{Si}_{33.4}$ ($\text{X} = \text{Fe}, \text{Mn}$), and $\text{Co}_{60.6}\text{Fe}_3\text{Mn}_3\text{Si}_{33.4}$, which were observed under a parallel magnetic field. All samples exhibit magnetic properties. Cristina Bormio-Nunes [13] studied the magnetisation of Co_2Si , which was obtained by heat treatment.

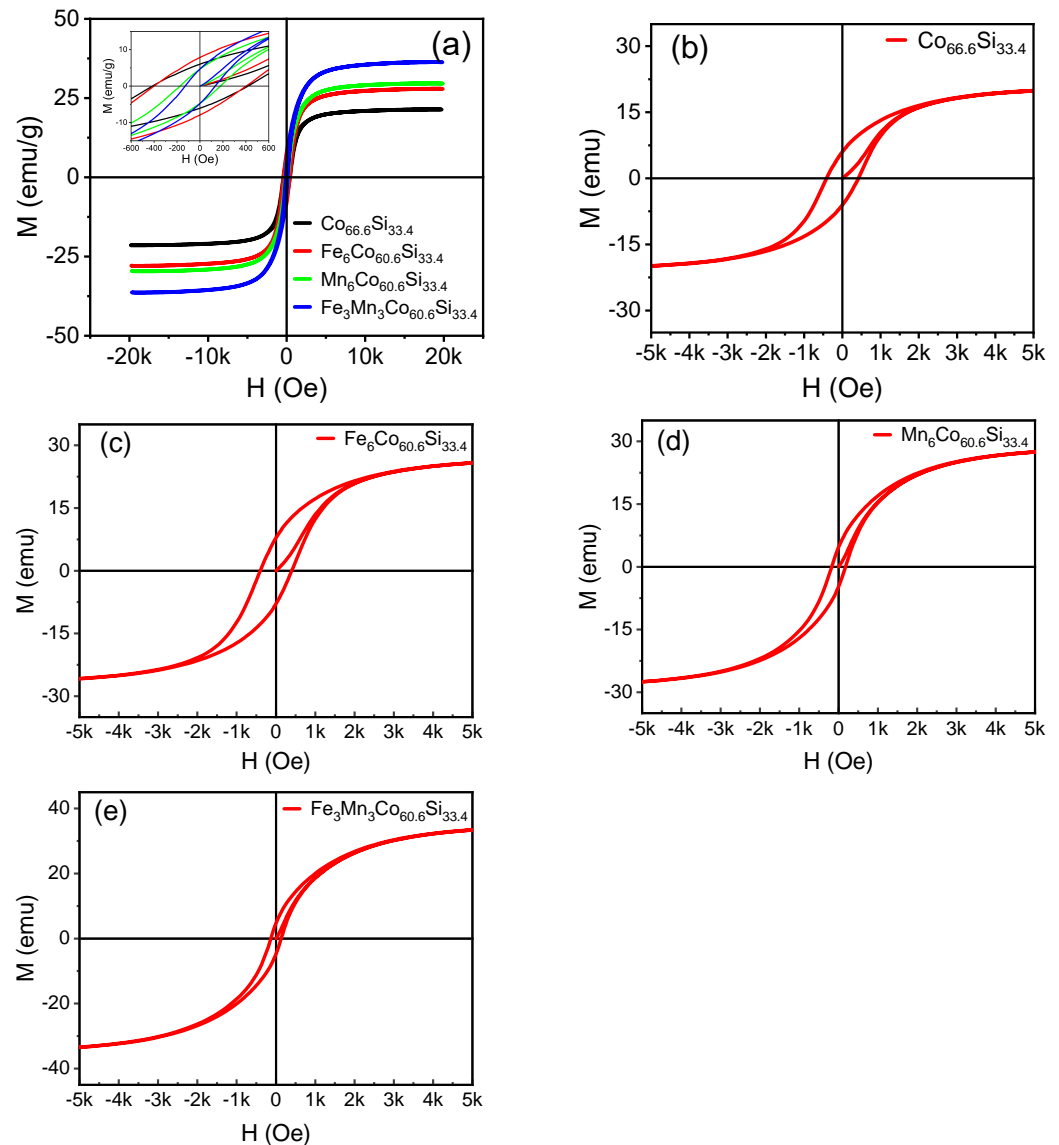


Figure 4. (a–e) Hysteresis loops of the as-prepared $\text{Co}_{66.6}\text{Si}_{33.4}$, $\text{Co}_{60.6}\text{X}_6\text{Si}_{33.4}$ ($\text{X} = \text{Fe}, \text{Mn}$), $\text{Co}_{60.6}\text{Fe}_3\text{Mn}_3\text{Si}_{33.4}$ samples sintered at 950 °C.

They obtained a saturation magnetisation of 18 kA/M, indicating that the magnetic properties are better than those obtained in our study. However, they performed powder heating at 1000 °C for 50 h, which requires complex instrumentation as Co_2Si is easily oxidised at high temperatures. Van der Walls-Zeeman [16] obtained Co_2Si by ball milling and sintering. They milled Co_2Si for 120, 260, and 629 h, then sintered it at 900 K. The diffraction peak matched the diffraction pattern of Co_2Si for the sample ball-milled for 629 h. However, the machine was continuously operated for hundreds of hours, resulting in damage to the mechanical bearing. Therefore, our method is more effective.

Table 3. Conductivities of as-prepared $\text{Co}_{66.6}\text{Si}_{33.4}$, $\text{Co}_{60.6}\text{X}_6\text{Si}_{33.4}$, ($\text{X} = \text{Fe}, \text{Mn}$), and $\text{Co}_{60.6}\text{Fe}_3\text{Mn}_3\text{Si}_{33.4}$.

Structure	$\text{Co}_{66.6}\text{Si}_{33.4}$	$\text{Fe}_6\text{Co}_{60.6}\text{Si}_{33.4}$	$\text{Mn}_6\text{Co}_{66.6}\text{Si}_{33.4}$	$\text{Fe}_3\text{Mn}_3\text{Co}_{60.6}\text{Si}_{33.4}$
1 MPa	280 (S/m)	297 (S/m)	30,002 (S/m)	17,500 (S/m)
2 MPa	512 (S/m)	649 (S/m)	68,900 (S/m)	24,300 (S/m)
3 MPa	183 (S/m)	190 (S/m)	111,000 (S/m)	32,000 (S/m)

Magnetisation gradually increases as increase in the magnetic field intensity (H); at a certain value, it attains saturation. The doping of $\text{Co}_{66.6}\text{Si}_{33.4}$ with Fe and Mn improved the saturation magnetisation of the sample. The obtained saturation magnetisations were 27.9, 29.6, and 36.3 emu/g. The magnetic moment of Co_2Si was significantly improved when $\text{Co}_{66.6}\text{Si}_{33.4}$ was doped with Fe and Mn, as inferred from theoretical analysis. By introducing different metal ions as dopants, the magnetism of $\text{Co}_{66.6}\text{Si}_{33.4}$ could be ameliorated.

The lattice will be changed during the introduction of ions, and in this process, some magnetic moments may be occur [27]. Consequently, the net magnetic moment of the sample increases and the macroscopic magnetism is enhanced. Following the introduction of Fe and Mn atoms into the lattice of $\text{Co}_{66.6}\text{Si}_{33.4}$, the orbit of Co is modified, and the hybridisation of the atomic orbital changes. After introducing the Fe and Mn dopants, the bond length changes, enhancing the magnetism. Figure 5 shows that the coercivity decreased after doping, and that of $\text{Co}_{60.6}\text{Fe}_3\text{Mn}_3\text{Si}_{33.4}$ reached a minimum value of 129.73 Oe.

These results show that the magnetic properties of $\text{Co}_{66.6}\text{Si}_{33.4}$ are enhanced after doping, and that the magnetic properties of $\text{Co}_{60.6}\text{Fe}_3\text{Mn}_3\text{Si}_{33.4}$ are excellent. The saturation magnetisation (M_s), coercivity (H_c), remanence magnetisation (M_r), and ratio of remanence to saturation magnetisation (M_r/M_s) of $\text{Co}_{60.6}\text{Fe}_3\text{Mn}_3\text{Si}_{33.4}$ are 36.3 emu/g, 129.73 Oe, 4.69 emu/g, and 0.16, respectively.

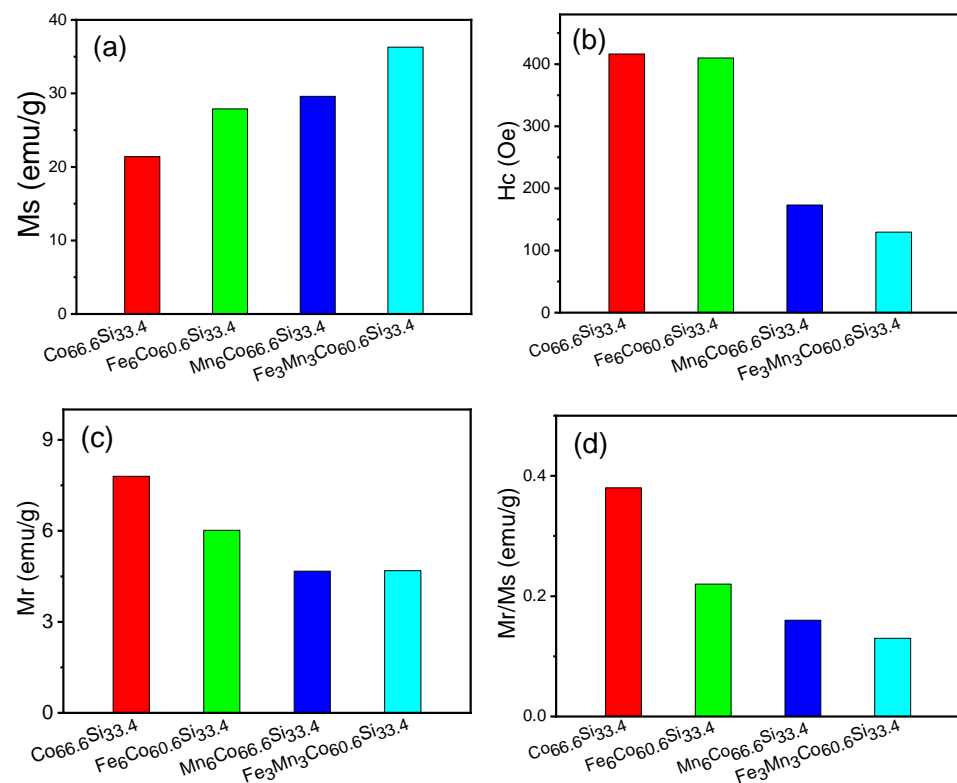
**Figure 5.** (a–d) M_s , H_c , M_r and M_r/M_s of as-prepared $\text{Co}_{66.6}\text{Si}_{33.4}$, $\text{Co}_{60.6}\text{X}_6\text{Si}_{33.4}$, ($\text{X} = \text{Fe}, \text{Mn}$), $\text{Co}_{60.6}\text{Fe}_3\text{Mn}_3\text{Si}_{33.4}$ samples.

Figure 5a–d shows the M_s , H_c , M_r , and M_r/M_s of all samples. The x-axis represents the type of material, namely $\text{Co}_{66.6}\text{Si}_{33.4}$, $\text{Co}_{60.6}\text{X}_6\text{Si}_{33.4}$, ($\text{X} = \text{Fe}, \text{Mn}$), or $\text{Co}_{60.6}\text{Fe}_3\text{Mn}_3\text{Si}_{33.4}$.

The y-axis shows the Ms, Hc, Mr, and Mr/Ms values, respectively. In Figure 5a, the Ms values of $\text{Co}_{66.6}\text{Si}_{33.4}$, $\text{Co}_{60.6}\text{X}_6\text{Si}_{33.4}$ (X = Fe, Mn), and $\text{Co}_{60.6}\text{Fe}_3\text{Mn}_3\text{Si}_{33.4}$ were 21.4, 27.9, 29.6, and 36.3 emu/g, respectively. Following doping, the magnetic saturation intensity improved, and that of $\text{Co}_{60.6}\text{Fe}_3\text{Mn}_3\text{Si}_{33.4}$ reaches the maximum value of 36.3 emu/g. When $\text{Co}_{66.6}\text{Si}_{33.4}$ is doped with Fe, the primary sources of magnetism are the d orbitals of Co and Fe; on the other hand, when $\text{Co}_{66.6}\text{Si}_{33.4}$ is doped with Mn, they are the d orbitals of Co and Mn.

The d orbital of Mn introduces a new magnetic source of magnetization atom, which enhances the coupling effect of the original system. When $\text{Co}_{66.6}\text{Si}_{33.4}$ is co-doped with Fe and Mn, the magnetic moment further increases, indicating that co-doping with Fe and Mn has a synergistic effect. Figure 5b compares the coercivities of $\text{Co}_{66.6}\text{Si}_{33.4}$, $\text{Co}_{60.6}\text{X}_6\text{Si}_{33.4}$ (X = Fe, Mn), and $\text{Co}_{60.6}\text{Fe}_3\text{Mn}_3\text{Si}_{33.4}$ with that of $\text{Co}_{66.6}\text{Si}_{33.4}$, and indicates that the samples underwent varying degrees of deterioration.

The coercivities of $\text{Co}_{66.6}\text{Si}_{33.4}$ and $\text{Co}_{60.6}\text{Fe}_3\text{Mn}_3\text{Si}_{33.4}$ were 173.4, and 129.73 Oe, respectively. The Hc of $\text{Co}_{60.6}\text{Fe}_3\text{Mn}_3\text{Si}_{33.4}$ was the lowest among all samples. In Figure 5c, the Mr values of $\text{Co}_{66.6}\text{Si}_{33.4}$, $\text{Co}_{60.6}\text{X}_6\text{Si}_{33.4}$ (X = Fe, Mn), and $\text{Co}_{60.6}\text{Fe}_3\text{Mn}_3\text{Si}_{33.4}$ exhibit slight differences. Further, the lower the Mr, the stronger the magnetic property. The Mr values of $\text{Co}_{66.6}\text{Si}_{33.4}$, $\text{Co}_{60.6}\text{X}_6\text{Si}_{33.4}$ (X = Fe, Mn), and $\text{Co}_{60.6}\text{Fe}_3\text{Mn}_3\text{Si}_{33.4}$ were 7.8, 6.02, 4.67, and 4.69 emu/g, respectively.

As shown in Figure 5d, the Mr/Ms ratios of $\text{Co}_{66.6}\text{Si}_{33.4}$, $\text{Co}_{60.6}\text{X}_6\text{Si}_{33.4}$ (X = Fe, Mn), and $\text{Co}_{60.6}\text{Fe}_3\text{Mn}_3\text{Si}_{33.4}$ were 0.38, 0.22, 0.16, and 0.13, respectively, exhibiting little in the way differences. In summary, the magnetic properties of $\text{Co}_{60.6}\text{Fe}_3\text{Mn}_3\text{Si}_{33.4}$ are significantly improved after doping; further, Co-doping had a significant effect on $\text{Co}_{60.6}\text{Fe}_3\text{Mn}_3\text{Si}_{33.4}$, whereby the saturation magnetisation reaches the maximum, its Hc was the lowest, and its Mr was remarkable.

Figure 6a,b, respectively, show the real (u') and imaginary permeabilities (u'') of $\text{Co}_{66.6}\text{Si}_{33.4}$, $\text{Co}_{60.6}\text{X}_6\text{Si}_{33.4}$ (X = Fe, Mn), and $\text{Co}_{60.6}\text{Fe}_3\text{Mn}_3\text{Si}_{33.4}$. Figure 6c,d, respectively, show the error bar of the real(u') and imaginary permeabilities (u'') of $\text{Co}_{66.6}\text{Si}_{33.4}$, $\text{Co}_{60.6}\text{X}_6\text{Si}_{33.4}$ (X = Fe, Mn), and $\text{Co}_{60.6}\text{Fe}_3\text{Mn}_3\text{Si}_{33.4}$ (mean \pm SD). The real permeability represents the storage capacity of magnetic energy, while the imaginary permeability reflects the ability to lose magnetic energy [28]. As shown in Figure 6a,b, we chose $\text{Co}_{66.6}\text{Si}_{33.4}$ as an example because they all had the same trend. The u' of $\text{Co}_{66.6}\text{Si}_{33.4}$ improved at 0.9–1.9 GHz, decreased at 1.9–2.68 GHz, and reached a maximum at the 1.9 GHz.

The u' of $\text{Co}_{66.6}\text{Si}_{33.4}$ fell and rose alternately, and there are ten peaks from 1.9 to 18 GHz. This figure shows a downward trend as a whole in the 1.9–18 GHz range. At 18–20 GHz, the permeability dropped to zero. The u'' of $\text{Co}_{66.6}\text{Si}_{33.4}$ started to appear at 1 GHz and reached its maximum immediately. Then it began to fall and reached 0 at 18 GHz.

As shown in Figure 6a,b, with increasing frequency, the u' and u'' of $\text{Co}_{66.6}\text{Si}_{33.4}$, $\text{Co}_{60.6}\text{X}_6\text{Si}_{33.4}$ (X = Fe, Mn), and $\text{Co}_{60.6}\text{Fe}_3\text{Mn}_3\text{Si}_{33.4}$ gradually decreased, indicating that the storage capacity of magnetic energy and the ability to lose magnetic energy decrease with increasing frequency.

At low frequencies, the u' and u'' of $\text{Co}_{66.6}\text{Si}_{33.4}$, $\text{Co}_{60.6}\text{Fe}_3\text{Mn}_3\text{Si}_{33.4}$ increase, whereas at high frequencies, after doping, they changed only slightly. This phenomenon indicates that doping has a greater effect on the properties in the low-frequency region than in the high-frequency region. As shown in Figure 6c,d, the maximum standard deviation of the u' of $\text{Co}_{66.6}\text{Si}_{33.4}$, $\text{Co}_{60.6}\text{X}_6\text{Si}_{33.4}$ (X = Fe, Mn), and $\text{Co}_{60.6}\text{Fe}_3\text{Mn}_3\text{Si}_{33.4}$ is, respectively, 0.03264, 0.06129, 0.0615, 0.0091.

The maximum standard deviation of the u'' of $\text{Co}_{66.6}\text{Si}_{33.4}$, $\text{Co}_{60.6}\text{X}_6\text{Si}_{33.4}$ (X = Fe, Mn), and $\text{Co}_{60.6}\text{Fe}_3\text{Mn}_3\text{Si}_{33.4}$ is, respectively, 0.03264, 0.06129, 0.0615, 0.0091. This is because we measured three times, and in the process of each measurement, we made a new loop, thus, resulting in a certain error.

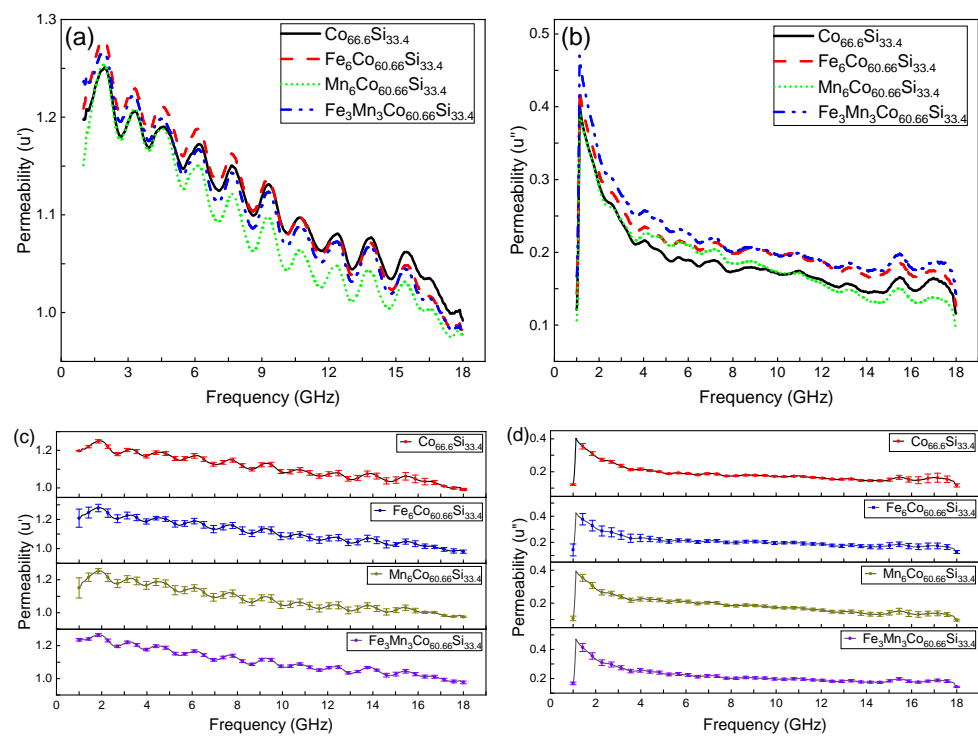


Figure 6. (a) Real permeability of $\text{Co}_{66.6}\text{Si}_{33.4}$, $\text{Co}_{60.6}\text{X}_6\text{Si}_{33.4}$, ($\text{X} = \text{Fe}, \text{Mn}$), and $\text{Co}_{60.6}\text{Fe}_3\text{Mn}_3\text{Si}_{33.4}$; (b) Imaginary permeability of $\text{Co}_{66.6}\text{Si}_{33.4}$, $\text{Co}_{60.6}\text{X}_6\text{Si}_{33.4}$, ($\text{X} = \text{Fe}, \text{Mn}$), and $\text{Co}_{60.6}\text{Fe}_3\text{Mn}_3\text{Si}_{33.4}$; (c) Real permeability of $\text{Co}_{66.6}\text{Si}_{33.4}$, $\text{Co}_{60.6}\text{X}_6\text{Si}_{33.4}$, ($\text{X} = \text{Fe}, \text{Mn}$), and $\text{Co}_{60.6}\text{Fe}_3\text{Mn}_3\text{Si}_{33.4}$ (mean \pm SD); (d) Imaginary permeability of $\text{Co}_{66.6}\text{Si}_{33.4}$, $\text{Co}_{60.6}\text{X}_6\text{Si}_{33.4}$, ($\text{X} = \text{Fe}, \text{Mn}$), and $\text{Co}_{60.6}\text{Fe}_3\text{Mn}_3\text{Si}_{33.4}$ (mean \pm SD).

4. Conclusions

In this study, the effects of different dopants on the crystal structure, electrical conductivity, and magnetic properties of Co_2Si were studied.

(1) Based on the PDF card (98-005-2281), a single phase of $\text{Co}_{66.6}\text{Si}_{33.4}$ was obtained by ball milling and sintering. The doped $\text{Co}_{66.6}\text{Si}_{33.4}$ did not form other phases, except for a phase of $\text{Co}_{66.6}\text{Si}_{33.4}$. There were slight differences between the measured and calculated grain sizes of $\text{Co}_{66.6}\text{Si}_{33.4}$, $\text{Co}_{60.6}\text{X}_6\text{Si}_{33.4}$, ($\text{X} = \text{Fe}, \text{Mn}$), and $\text{Co}_{60.6}\text{Fe}_3\text{Mn}_3\text{Si}_{33.4}$ (measured: 23, 21, 38, and 32 nm, respectively; calculated: 36.8, 34.4, 46.8, and 45.8 nm, respectively). This is due to the different methods employed (the data of XRD for calculation for calculation and TEM for measurements). Another reason is that magnetic materials affect the accuracy of the measured grain sizes.

(2) Under pressures of 1, 2, and 3 MPa, the resistivity of each samples was measured by a resistance meter. The conductivity was calculated by taking the reciprocals of resistivities. The effect of Fe doping on the conductivity was insignificant. The conductivities of $\text{Mn}_6\text{Co}_{60.6}\text{Si}_{33.4}$ and $\text{Fe}_3\text{Mn}_3\text{Co}_{60.6}\text{Si}_{33.4}$ were superior to that of $\text{Co}_{66.6}\text{Si}_{33.4}$, indicating that the doping of Mn atoms has an influence on the electronic structure. This is because the entry of Mn atoms enhanced the electron mobility.

(3) The $\text{Co}_{66.6}\text{Si}_{33.4}$ alloy exhibited typical magnetic properties, which were improved after doping. At the same temperature, M_s increased, whereas H_c , M_r , and M_r/M_s decreased. This indicates that the magnetic properties of the $\text{Co}_{66.6}\text{Si}_{33.4}$ alloy are ameliorated after doping. Among the doping strategies employed, the effect of the co-doping of Fe and Mn was excellent, the resulting values of M_s , H_c , M_r , and M_r/M_s were 36.3 emu/g, 129.73 Oe, 4.69 emu/g, and 0.16, respectively.

(4) The storage capacity of magnetic energy and the ability to lose magnetic energy declined with increasing frequency for $\text{Co}_{66.6}\text{Si}_{33.4}$ and doped $\text{Co}_{66.6}\text{Si}_{33.4}$. This is because impedance matching also plays a role. If the impedance does not match, lesser electromagnetic waves will enter the material, resulting in no improvement in the storage capacity

despite a decrease in the loss of magnetic energy. Doping affects the permeability in the low-frequency region more than in the high-frequency region.

(5) This work suggests alternative candidates for future magnetic functional materials. The low coercivities of $\text{Mn}_6\text{Co}_{60.6}\text{Si}_{33.44}$ and $\text{Fe}_3\text{Mn}_3\text{Co}_{60.6}\text{Si}_{33.4}$ render them promising for use as audio and video magnetic head materials. The remanence characteristics of doped $\text{Co}_{66.6}\text{Si}_{33.4}$ may render it suitable for use in electronic transformers.

Author Contributions: Methodology, J.Z. and Q.X.; software, L.W., B.W. and J.H.; data curation, J.Z. and L.W.; writing-original draft preparation, J.Z. and Q.X.; writing-review and editing, J.Z., L.W. and Q.X. All authors have read and agreed to the published version of the manuscript

Funding: The study was supported by the Industry and Education Combination Innovation Platform of Intelligent Manufacturing and Graduate Joint Training Base at Guizhou University (Grant No: 2020-520000-83-01-324061), the National Natural Science Foundation of China (Grant No.61264004), and High-level Creative Talent Training Program in Guizhou Province of China (Grant No. [2015]4015). The Education Department of Guizhou Province Electronic Manufacturing Production Base (NO. [2014]230).

Data Availability Statement: The data presented in this study are available on request from the corresponding author.

Conflicts of Interest: The authors declare no conflict of interest. The authors claim that none of the material in our manuscript has been published or is under consideration for publication elsewhere. This manuscript is our original work.

References

- Zhiyao, J.; Yue, M.; Qing W.; Chuang, D. Research progress on high performance soft-magnetic alloys. *J. Mater. Eng.* **2021**, *299*, 1–18.
- Bin, J.; Wei, W. Research Progress in Electrochemical Synthesis of Fe-based Soft Magnetic Films. *Surf. Technol.* **2021**, *50*, 151–158.
- Liu, J.; Mei, Y.; Lu, G. Development of High-frequency Soft Magnetic Materials for Power Electronics. *J. Mater. Eng.* **2017**, *45*, 127–134.
- Huang, M.; Wu, K.; Xiang, Q.; Zhang, K.; Tsepelev, V.S.; Wang, R. Research status and future development trend of a novel FeSiBPCu nano soft magnetic alloy. *J. Iron Steel Res.* **2018**, *30*, 763–768.
- Barth, M.; Wei, B.; Herlach, D.M. Crystal-growth in undercooled melts of the intermetallic compounds FeSi and CoSi. *Phys. Rev. B* **1995**, *51*, 3422–3428. [[CrossRef](#)] [[PubMed](#)]
- Tao, Z.X.; Li, L.Z.; Wu, X.H.; Zhong, X.X.; Zhong, Z.C. Structural, magnetic and electrical properties of CoSi ferrites synthesized by sol-gel self-propagating method. *Phys. B-Condens. Matter* **2021**, *604*. [[CrossRef](#)]
- Chengchuan, L.I.; Weili, R.E.N.; Zhijun, P.A.N.; Lanting, Z.; Jiansheng, W.U. The synthesis of thermoelectric compound CoSi by mechanical alloying. *J. Shanghai Jiaotong Univ.* **2006**, *40*, 889–892.
- Pan, Z.J.; Zhang, L.T.; Wu, J.S. First-principles study of electronic structure for CoSi. *Acta Phys. Sin.* **2005**, *54*, 328–332.
- Jo, C.; Kim, D.C.; Lee, J.I. Magnetic properties of Co-Si alloy clusters. *J. Magn. Magn. Mater.* **2006**, *306*, 156–160. [[CrossRef](#)]
- Velez, M.; Valvidares, S.; Diaz, J.; Morales, R.; Alameda, J. Structure and magnetic properties of amorphous CoSi alloy films. *IEEE Trans. Magn.* **2002**, *38*, 3078–3080. [[CrossRef](#)]
- Geller, S. The crystal structure of Co_2Si . *Acta Crystallogr.* **1955**, *8*, 83–87. [[CrossRef](#)]
- Jan, C.H.; Chen, C.P.; Chang, Y.A. Growth of intermediate phases in Co/Si diffusion couples-Bulk versus thin-film studies. *J. Appl. Phys.* **1993**, *73*, 1168–1179. [[CrossRef](#)]
- Bormio-Nunes, C.; Nunes, C.A.; Coelho, A.A.; Sodero Toledo Faria, M.I.; Suzuki, P.A.; Coelho, G.C. Magnetization studies of binary and ternary Co-rich phases of the Co-Si-B system. *J. Alloys Compd.* **2010**, *508*, 5–8. [[CrossRef](#)]
- Tu, K.N.; Ottaviani, G.; Thompson, R.D.; Mayer, J.W. Thermal-stability and growth-kinetics of Co_2Si and CoSi in thin-film reactions. *J. Appl. Phys.* **1982**, *53*, 4406–4410. [[CrossRef](#)]
- Baldan, R.; Sodero Toledo Faria, M.I.; Nunes, C.A.; Coelho, G.C.; Chad, V.M.; de Avillez, R.R. Microstructural Evidence of beta Co_2Si -phase Stability in the Co-Si System. *J. Phase Equilibria Diffus.* **2008**, *29*, 477–481. [[CrossRef](#)]
- Zhou, G.F.; Bakker, H. Atomically disordered nanocrystalline Co_2Si by high-energy ball-milling. *J.-Phys.-Condens. Matter* **1994**, *6*, 4043–4052. [[CrossRef](#)]
- Chen, X.; Huang, H.; Li, F. Phase transformation in $\beta\text{-FeSi}_2$ thermoelectric materials during mechanical alloying and heat-treatment. *J. Southeast Univ. Nat. Sci. Ed.* **2008**, *38*, 898–901.
- Zhang, X.; Ma, R.; Xie, Q. Effects of Ni doping amount on microwave absorptive properties of Fe_3Si alloy. *Electron. Compon. Mater.* **2014**, *33*, 38–41.
- Chen, Z.; Zhang, J.; Zhao, Q.; Zhu, P.; Zheng, X.; Xie, Q. Preparation of intermetallic compound Fe_3Si with mechanical alloying and hot-pressing sintering. *J. Mater. Sci. Eng.* **2012**, *30*, 442–448.

20. Lee, Y.; Jeon, J.K.; Shin, H.; Kim, J.Y. Magnetic behaviors of $\text{Ti}_{50}\text{Zr}_{33}\text{Ni}_{17}$ quasicrystals measured by VSM. *Z. Fur Krist.* **2009**, *224*, 67–70. [[CrossRef](#)]
21. He, H.Y.; Huang, J.F.; Cao, L.Y.; He, Z.; Shen, Q. Magnetic and microwave-absorbing properties of $\text{SrAl}_4\text{Fe}_8\text{O}_{19}$ powders synthesized by coprecipitation and citric-combustion methods. *Bull. Mater. Sci.* **2011**, *34*, 463–468. [[CrossRef](#)]
22. Brazhkin, V.V.; Bychkov, E.; Tsiok, O.B. High-precision measurements of the compressibility and the electrical resistivity of bulk $\text{g-As}_2\text{Te}_3$ glasses at a hydrostatic pressure up to 8.5 GPa. *J. Exp. Theor. Phys.* **2017**, *125*, 451–464. [[CrossRef](#)]
23. Zhong, Y.; Ping, D.; Song, X.; Yin, F. Determination of grain size by XRD profile analysis and TEM counting in nano-structured Cu. *J. Alloys Compd.* **2009**, *476*, 113–117. [[CrossRef](#)]
24. Jianxin, L.; Dangyu, S.; Junying, Z.; Chuguang, Z. Evaluation of the X-ray Diffraction Data Analysis System. *Rock Miner. Anal.* **2008**, *27*, 189–192. 196.
25. Velde, H.; Platbrood, G. Detectability of two overlapping Pearson VII peaks in simulated X-ray diffraction patterns. *Int. Union Crystallogr.* **1985**, *18*, 114–119. [[CrossRef](#)]
26. Zak, A.K.; Majid, W.H.A.; Abrishami, M.E.; Yousefi, R. X-ray analysis of ZnO nanoparticles by Williamson–Hall and size-strain plot methods. *Solid State Sci.* **2011**, *13*, 251–256.
27. Ul Haque, S.; Saikia, K.K.; Murugesan, G.; Kalainathan, S. A study on dielectric and magnetic properties of lanthanum substituted cobalt ferrite. *J. Alloys Compd.* **2017**, *701*, 612–618. [[CrossRef](#)]
28. Xiong, Y.; Xu, L.; Yang, C.; Sun, Q.; Xu, X. Implanting FeCo/C nanocages with tunable electromagnetic parameters in anisotropic wood carbon aerogels for efficient microwave absorption. *J. Mater. Chem. A* **2020**, *8*, 18863–18871. [[CrossRef](#)]